In-Situ X-ray Spectroscopy of the Electric Double Layer around TiO$_2$ Nanoparticles Dispersed in Aqueous Solution: Implications for H$_2$ Generation

Hebatallah Ali,*[†,‡] Ronny Golnak,[§] Robert Seidel,[∥,⊥] Bernd Winter,[†] and Jie Xiao*[§]

[†]Department of Molecular Physics, Fritz-Haber-Institut der Max-Planck-Gesellschaft, Faradayweg 4-6, D-14195 Berlin, Germany
[‡]Fachbereich Physik, Freie Universität Berlin, Arnimallee 14, D-14195 Berlin, Germany
[§]Department of Highly Sensitive X-ray Spectroscopy and [∥]Department of Operando Interfacial Photochemistry, Helmholtz-Zentrum Berlin für Materialien und Energie, Albert-Einstein-Straße 15, D-12489 Berlin, Germany
[⊥]Department of Chemistry, Humboldt-Universität zu Berlin, Brook-Taylor-Straße 2, D-12489 Berlin, Germany

Ⓢ *Supporting Information*

ABSTRACT: We report an experimental observation of a significant amount of hydroxide (OH$^-$) created upon water dissociation and subsequently trapped around TiO$_2$ nanoparticles dispersed in NH$_4$OH aqueous solution. The hydroxide species is identified and quantified by a combination of photoemission and photon emission X-ray spectroscopies conducted on liquid samples using a liquid microjet. Unlike previous X-ray studies that observed only a few monolayers of water coverage on TiO$_2$ surfaces and found maximally submonolayer of OH$^-$, the true aqueous environment adopted in this study enables ion mobility and the separation of the water dissociation products H$^+$/OH$^-$. This facilitates the formation of OH$^-$ diffused multilayer in which the trapped OH$^-$ ions are discovered to coordinate with three water molecules to form a tetrahedral hydration configuration. The negatively charged diffuse layers, together with the positive NH$_4^+$ Stern layers, constitute >0.8 nm thick electric double layers around the TiO$_2$ nanoparticles. The large observed amount of hydroxide indicates a high efficiency of water dissociation for the TiO$_2$ catalyst, a promising result for H$_2$ generation in true aqueous environments.

KEYWORDS: electric double layer, TiO$_2$ nanoparticles, water dissociation, liquid microjet, photoelectron spectroscopy, X-ray absorption spectroscopy
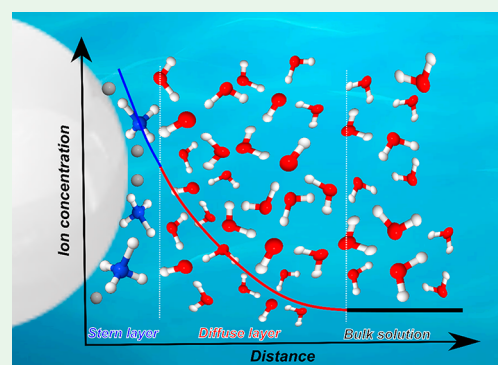
INTRODUCTION

Titanium dioxide (TiO$_2$) is a promising material to catalyze water dissociation for the production of H$_2$ fuel as a clean and renewable energy source.[1−5] Among the three TiO$_2$ phases, brooktile, rutile, and anatase, the latter phase exhibits the highest photocatalytic activity[6,7] and chemical stability in various aqueous environments.[8] Many efforts have been made to improve the TiO$_2$-catalyzed energy conversion efficiency in water-splitting reactions.[3,4,9−14] However, the fast back-reaction of proton (H$^+$) and hydroxide (OH$^-$) recombination into water molecules reduces the efficiency significantly.[5] The spatial separation of a proton from a hydroxide is therefore very critical for the enhancement of the water dissociation efficiency and for the device performance. This separation of the dissociation products, H$^+$ and OH$^-$ ions, in the vicinity of the TiO$_2$−water interface requires a true aqueous environment (rather than a few monolayers of water coverage) to enable ions to diffuse away from the interface. In fact, the electric double layer (EDL) that forms at the TiO$_2$−water interface will strongly influence ion distributions and ion mobilities.

Several models have been proposed to describe the EDL, including the Helmholtz model,[15] the Gouy−Chapman model,[16,17] and the Gouy−Chapman−Stern model.[18] In the Helmholtz model, the EDL is treated analogously to a static electric capacitor[19,20] where all counterions are postulated to be confined at the TiO$_2$ surface, and all co-ions are repelled. The ion mobility in the solution is completely ignored in this model.[19,20] It is, however, taken into account in the Gouy−Chapman model that postulates an interfacial diffuse layer where the ion concentration follows a Boltzmann distribution away from the interface.[20] This model assumes that ions are point charges and occupy no space, which can lead to an overestimation of surface charge.[20] The Gouy−Chapman−Stern model,[18] based on the two previous models, introduces an additional layer: the Stern layer where some or all counterions are confined at the TiO$_2$ surface. The remaining
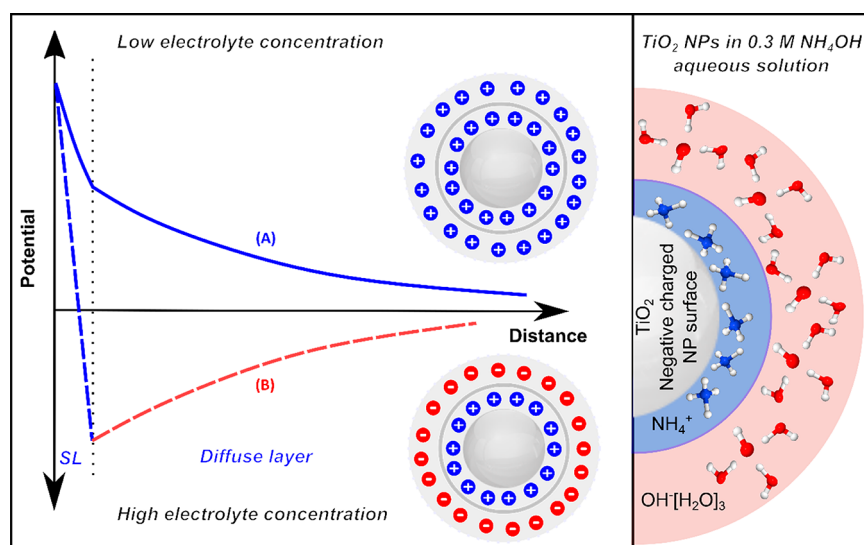
Figure 1. Left panel: potential curves of the EDL surrounding the nanoparticle: (A) low electrolyte concentration and (B) high electrolyte concentration (adsorbing counterions) leading to charge reversal. The figure is partially adapted from ref 21. Right panel: the structure and chemical composition of the formed electric double layer around titanium dioxide nanoparticles dispersed in highly concentrated electrolyte aqueous solution (0.3 M NH$_4$OH) is schematically illustrated.

counterions or co-ions, depending on the electrolyte concentration, are mobile and form the diffuse layer.[21] As in the Gouy–Chapman model, ions follow a Boltzmann distribution across the layer. The thickness of the EDL in the Gouy–Chapman–Stern model is defined as the Debye length, which is strongly dependent on the electrolyte concentration.[19] In this study, the Gouy–Chapman–Stern model is most appropriate for an analysis of the acquired spectra.

Although the charge parity of the EDL at the TiO$_2$–water interface in a dilute aqueous solution has been extensively investigated by various methods,[22−25] we still lack a quantitative molecular-level experimental insight into the detailed EDL structure, including the Debye length (electrostatic screening length). Soft X-ray spectroscopy studies that can directly reveal element-specific electronic structure of interfacial species are still scarce for solid surfaces in contact with real (bulk) aqueous solution. In recent years, the development of ambient pressure X-ray photoelectron spectroscopy (AP-PES) has allowed for instance probing of the EDL of a thin electrolyte film on top of a polycrystalline gold electrode created by the so-called "dip-and-pull method" by using tender X-ray radiation.[26] In the aforementioned study, the Debye length, measured as a function of the KOH electrolyte concentration, has been reported to decrease monotonically from 30.4 nm at 0.1 mM to ∼1.9 nm at near 80 mM concentration.[26] Despite extensive experimental efforts, PES studies seeking to reveal the EDL dimension have remained limited to nanometers thick water coverage, in which case ion mobility and ion adsorption/desorption at the TiO$_2$ surface will be different than in bulk solution.[27] In-situ probing of the TiO$_2$ surface fully immersed in liquid water is therefore of great importance despite the experimental challenges it poses.

In this study, X-ray photoelectron spectroscopy (XPS) and partial electron/fluorescence yield X-ray absorption spectroscopy (PEY/PFY-XAS) measurements were conducted on anatase-phase TiO$_2$ nanoparticles (NPs) dispersed in slightly basic aqueous NH$_4$OH solution (pH ∼7.8). We have recently

demonstrated dissociative water adsorption at the NP–solution interface in such a TiO$_2$ system.[28] Here, we report complementary electron-yield and photon-yield detections to quantify the amount of water dissociation at the TiO$_2$–water interface as well as to estimate the Debye length. The NP solution has a concentration of 20 wt % corresponding to an average separation distance between the dispersed NPs of ∼80 μm. In this case of high NP concentration, the Stern layer is composed of stabilizer NH$_4^+$ ions (discussed later with Figure 2). The stable NP solution (with no aggregation) can be well described by the Derjaguin, Landau, Verwey, and Overbeek (DLVO) theory.[19,20] At high electrolyte concentration, the NP interaction potential barrier is lowered, and a minimum in the potential curve (a secondary energy barrier with oppositely charged ions) can lead to slow NP aggregation.[20] For electrolyte concentrations above the so-called critical coagulation value, the energy barrier reduces to below zero and triggers NPs to aggregate rapidly.[20] The TiO$_2$ NP colloidal solution in this study is of relatively high concentration but is still below the critical value. We briefly review the expected nature of the EDL and how it depends on the electrolyte concentration. As illustrated in curve A of the left panel of Figure 1, at low electrolyte concentration, positive charge (NH$_4^+$ cations) accumulates at the NP surface to establish charge neutrality of the NP + EDL entity. Curve B of the left panel of Figure 1 shows how at high electrolyte concentrations, negative charge from the electrolyte (OH$^−$ in our case) will be drawn closer to the NPs and stay associated with them throughout the EDL (Figure 1, right panel). The primary goal of the present study is to use PES together with the more bulk-sensitive PFY-XA spectroscopy to identify the molecular nature of the EDL, including the quantity and composition of oppositely charged ions, and to estimate the thickness of the EDL and infer hydration structure details. Our finding of a large quantity of hydroxides around the TiO$_2$ NPs not only indicates efficient water dissociation reactions catalyzed by TiO$_2$ NPs but also points at an efficient pathway for H$_2$ generation catalyzed by TiO$_2$ surfaces in aqueous solutions.
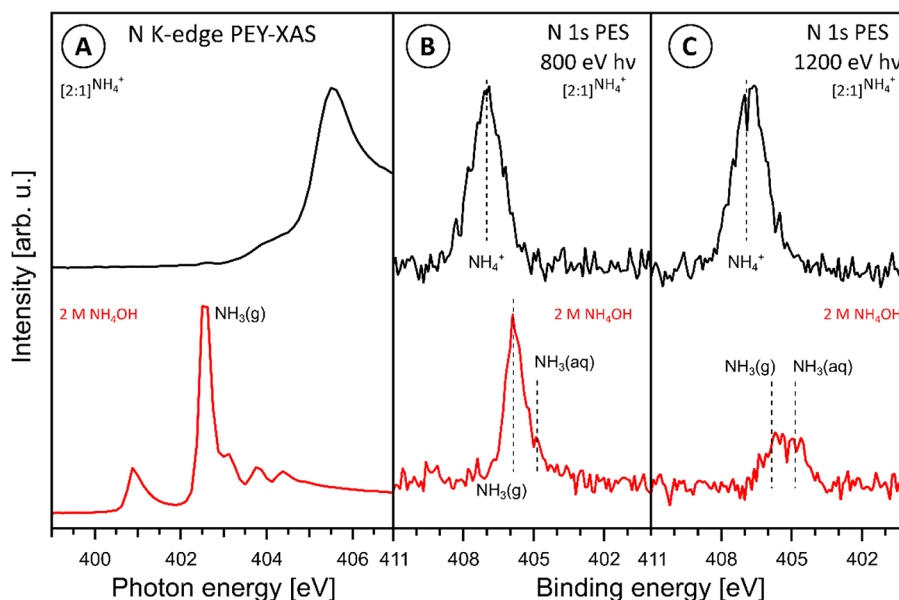
Figure 2. (A) Nitrogen K-edge PEY-XA spectra from $[2:1]^{NH_4^+}$ NP (black, top) and 2 M NH_4OH (red, bottom) aqueous solutions and the respective N 1s photoelectron spectra measured at 800 eV (B) and 1200 eV (C) photon energies. Spectral contributions of $NH_3(g)$, $NH_3(aq)$, and NH_4^+ are labeled.

■ EXPERIMENTAL SECTION

Both the PES and PEY-XAS measurements were conducted with the SOL^{3}PES setup,[29] and the PFY-XAS studies were performed with the LiXedrom setup,[30] at the synchrotron-radiation facility BESSY II, Berlin. For all measurements we used the soft X-ray beamline U49/2-PGM1. A 20 wt % colloidal solution of 20 nm diameter anatase-phase TiO_2 NPs dispersed in 0.3 M NH_4OH aqueous solution was acquired from NYACOL, USA, and introduced into the experimental vacuum chambers via a liquid microjet.[31] We also investigated 0.5 and 2 M NH_4OH and 5 M NaOH aqueous solutions (prepared by using ammonium hydroxide solution—28% NH_3 in H_2O, >99.99% purity, and sodium hydroxide, >97.0% purity, provided from Sigma-Aldrich (Merck)) as well as a 20 wt % colloidal solution of 10 nm diameter anatase-phase TiO_2 NPs (>99.9% purity) dispersed in 0.5 M HCl aqueous solution purchased from MK Nano, Canada—all of which served as spectral references. Note that the NP surface in 0.5 M HCl aqueous solution is fully covered by adsorbed Cl^- ions, so water cannot interact with the TiO_2 NP. This provides a useful spectroscopic reference and has been applied in several previous liquid microjet PES studies.[29,32−36] According to the concentrations of the TiO_2 NP (20 wt %) and NH_4OH (0.3 M) aqueous solutions, the NP diameter (20 nm), and with the reported adsorption density of ~5.2 molecules/nm^2 on the TiO_2 surface,[37,38] we estimate that approximately half of the total NP surface is covered by NH_4^+ stabilizer ions. This leaves the other half of TiO_2 surface sites available for the interaction with water. In the following, the term $[X:Y]^{st}$ is used to indicate the ratio between the available TiO_2 surface sites X and adsorbed stabilizer ions Y where "st" denotes the stabilizer ion. As such, $[2:1]^{NH_4^+}$ and $[1:1]^{Cl^-}$ denote the NP solutions where half of the NP surface is covered by NH_4^+ and fully covered by Cl^- ions, respectively.

■ RESULTS AND DISCUSSION

In an ammonia aqueous solution, hydrated ammonia under-goes a chemical equilibrium reaction with liquid water

$$NH_3(aq) + H_2O \leftrightarrow NH_4^+(aq) + OH^- \qquad (1)$$
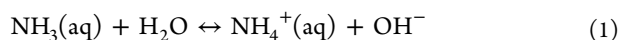
making the solution basic. This reaction is dependent on temperature and pH, and an equilibrium between NH_3 and NH_4^+ species is established at approximately pH 9 ($pK_a \sim 9$)

at 24 °C.[39,40] A 0.3 M NH_4OH aqueous solution (containing no TiO_2 NPs) has pH 11.3. When TiO_2 NPs are dispersed into the solution, NH_4^+ stabilizer ions adsorb at the NP surface[19] (see Figure 1, right panel), and as a result, there is no free NH_4^+ in the solution. NH_4^+ adsorption thus perturbs the ammonium−ammonia chemical equilibrium (eq 1) and leads to the production of more OH^-. However, the experimentally measured pH of the $[2:1]^{NH_4^+}$ NP colloidal solution is 7.8, just slightly above neutral pH. This surprising observation implies the presence of additional reactions other than the ammonium−ammonia equilibrium that occur in the solution and affect the number of free OH^- ions. To determine these additional reactions, we first investigate NH_4^+ ions in the presence of TiO_2 NPs and subsequently compare with NH_4OH aqueous solution (without TiO_2 NPs added) by measuring the PEY-XA at the N K-edge and XP spectra of the N 1s orbital. We then explore the OH^- species by recording the O 1s XP spectra from the 5 M NaOH, 0.5 M NH_4OH, $[2:1]^{NH_4^+}$ NP aqueous solutions and $[2:1]^{NH_4^+}$ NP aqueous solution with 0.5 M NaOH added. Finally, we derive the hydroxide hydration configuration for the $[2:1]^{NH_4^+}$ NP aqueous solution based on its O K-edge PFY-XA spectrum in comparison with the reference spectra of $[1:1]^{Cl^-}$ NP and 1.5 M NaOH aqueous solutions.

Figure 2A shows the N K-edge PEY-XA spectra of the $[2:1]^{NH_4^+}$ NP solution and 2 M NH_4OH aqueous solution (pH ~12). These two spectra are generated by integrating the signal intensity of the valence-band photoelectron spectra (not shown here) as a function of photon energy; see, e.g., ref 41 for a more detailed explanation. Observed spectral differences reveal the existence of different nitrogen-containing species in the two solutions. The spectrum of the 2 M NH_4OH solution (Figure 2A, bottom) primarily exhibits spectral features characteristic of neutral gas-phase ammonia (NH_3).[42] This can be explained by the ammonium−ammonia equilibrium reaction (eq 1). At high pH ~12, the equilibrium reaction

moves toward the $NH_3(aq)$ side; because of ammonia's high volatility[39,40] and the rather short probing depth of soft X-ray PES, the spectrum is then dominated by the $NH_3(g)$ signal. Note that Henry's constant for the hydrated NH_3 is relatively high, 59 mol/atm at 25 °C.[43] Under the experimental conditions, we expect $NH_3(aq)$ to be below the detection limit—this is confirmed by the absence of the main feature that would be expected to appear between the first two peaks of gas phase followed by an intense absorption step edge,[42] clearly not present in the bottom spectrum of Figure 2A. Our observation is in agreement with a previous N 1s Auger electron/autoionization PE study from a 2.6 M NH_3 aqueous solution.[44] Turning now to the N K-edge PEY-XA spectrum of the $[2:1]^{NH_4^+}$ NP solution (Figure 2A, top), we find reasonable resemblance to the reported spectrum of a NH_4^+ aqueous solution,[43] but a better agreement is obtained when comparing to the dry NH_4^+ salts.[45,46] Considering the nearly neutral pH of this solution, it suggests that NH_4^+ ions are adsorbed at the TiO_2 NP surfaces, acting as a stabilizer.

Our conclusion on the nature of the nitrogen-containing species is corroborated by the N 1s XP spectra from the same two solutions, also presented in Figure 2. Measurements were performed at two photon energies: 800 eV (Figure 2B) and 1200 eV (Figure 2C). The latter energy probes deeper into the solutions due to the larger kinetic energies (KE) of the photoelectrons.[47] Beginning with the 800 eV spectrum taken from the 2 M NH_4OH solution (Figure 2B, bottom), we observe a large peak at 405.9 eV binding energy (BE) arising from N 1s ionization of gas-phase ammonia, $NH_3(g)$. The signal from $NH_3(aq)$ is weak, giving rise to a small shoulder at 404.8 eV BE. In contrast, the 800 eV PE spectrum of the $[2:1]^{NH_4^+}$ NP solution (Figure 2B, top) exhibits a single peak at larger BE of 407.0 eV originating from N 1s ionization of adsorbed ammonium stabilizer, NH_4^+. This is exactly what we would expect from Figure 2A, top. Note also that in both cases the energies of the detected electrons are rather similar. That is, the KEs of the N 1s photoelectrons (excited by 800 eV photon energy) and of the N 1s Auger electrons (from which the PEY-XA spectrum in Figure 2A, bottom, has been obtained) are ~400 eV. At this energy the electron probing depth is thus too small to detect a noticeable signal from $NH_3(aq)$. Increasing the photon energy from 800 to 1200 eV has a minor effect on the XP spectrum of $[2:1]^{NH_4^+}$ solution (Figure 2C, top), but one observes a drastic change of the spectrum from the 2 M NH_4OH solution (Figure 2C, bottom). Because of the increased probing depth, the spectrum of the 2 M NH_4OH solution now exhibits, in addition to the $NH_3(g)$ signal at 405.9 eV, a second peak at 404.8 eV of similar intensity arising from $NH_3(aq)$. This implies that the majority of NH_4^+ in the $[2:1]^{NH_4^+}$ NP solution cannot be assigned to species solvated in bulk solution. If this were the case, a significant amount of $NH_3(g)$ (and some $NH_3(aq)$ at 1200 eV excitation energy) signal would be detected due to the ammonia–ammonium equilibrium (eq 1). Therefore, Figure 2 reveals that almost all NH_4^+ ions in the $[2:1]^{NH_4^+}$ NP solution are adsorbed on the TiO_2 NP surface, covering about half of the available surface area, as mentioned above. The adsorbed NH_4^+ ions constitute a positively charged Stern layer of the EDL. The thickness of this Stern layer is on the order of the diameter of the NH_4^+ ion which is ~0.35 nm, assuming a 0.175 nm NH_4^+ ionic radius.[48]

We next focus on the nature of the oxygen-containing species, with a particular interest in identifying dissociated water and estimating the amount of OH^- anions, which allows for an approximation of the length of the diffuse layer. For this we have measured the oxygen 1s PE (Figure 3) and oxygen K-
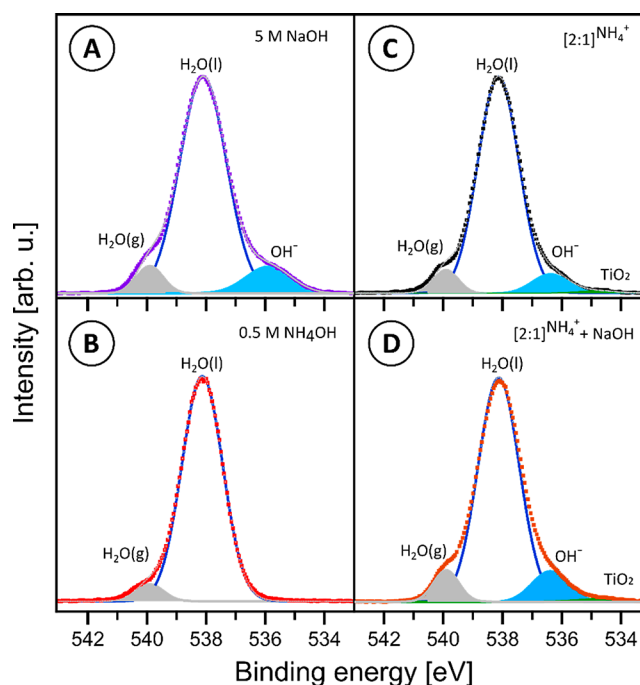
Figure 3. O 1s PE spectra of 5 M NaOH (A), 0.5 M NH_4OH (taken from ref 28) (B), $[2:1]^{NH_4^+}$ NP (taken from ref 28) (C), and $[2:1]^{NH_4^+}$ NP + 0.5 M NaOH (D) aqueous solutions measured at 1200 eV photon energy. Note that solution in (D) has pH of only 9.8, whereas the pure 0.5 M NaOH solution has pH 13.7. All spectra are fitted with multiple Gaussian functions that each represent the different oxygen species: liquid water ($H_2O(l)$), gas-phase water ($H_2O(g)$), OH^-, and TiO_2. Spectra are presented on the binding energy scale, and intensities of the different spectra are displayed to yield the same peak height of the liquid-water peak. Dots are the measured data, and the solid red lines are the total fits. The detailed fitting parameters are presented in Table S1.

edge PFY-XA (Figure 4) spectra from the same $[2:1]^{NH_4^+}$ NP solution. In addition, we present the respective spectra from two reference aqueous solutions: 5 M NaOH and 0.5 M NH_4OH. The 5 M NaOH solution is used to establish the OH^- PES peak position and to identify the effect of OH^- on the water structure through changes of the water O 1s PE peak. Note that 0.5 M concentration is reasonably close to the 0.3 M NH_4OH concentration used to stabilize the aqueous-phase TiO_2 NPs. All PE spectra were measured at 1200 eV photon energy, at the same energy which we have applied to increase the probing depth into the solution in the case of the N 1s PE measurements (Figure 2C). Figure 3A shows the O 1s PE spectrum from the 5 M NaOH aqueous solution. Three major oxygen features can be observed: the dominating liquid-water peak at 538.1 eV BE,[31] the water-vapor contribution at 539.9 eV,[49,50] and the hydrated OH^- giving rise to a shoulder at 535.8 eV.[51] These contributions are highlighted by the respective Gaussian fits shown in different colors (see Figure 3 caption for details). The O 1s PE spectrum from the other reference solution, 0.5 M NH_4OH, shown in Figure 3B
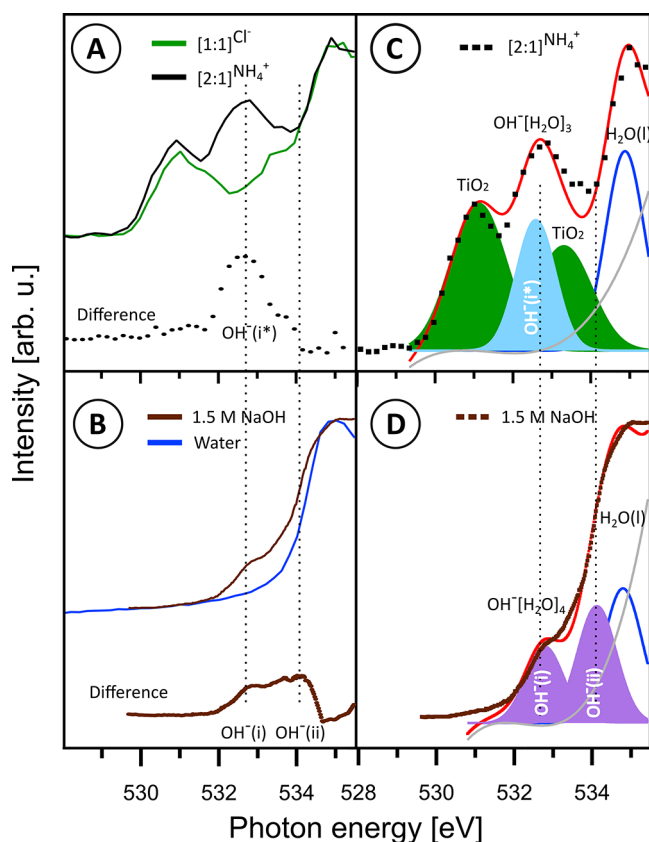
Figure 4. O K-edge PFY-XA spectra from $[2:1]^{NH_4^+}$ NP and $[1:1]^{Cl^-}$ NP aqueous solutions, along with the respective spectral difference (A), and from 1.5 M NaOH aqueous solution (taken from ref 54) and neat liquid water as well as their spectral difference (B). In (A) and (B) intensities are normalized at the water pre-edge. The Gaussian fits of the $[2:1]^{NH_4^+}$ NP and 1.5 M NaOH solution spectra are presented in (C) and (D), respectively. Different filling colors refer to different oxygen species: liquid-water oxygen (no filling), gas-phase water (gray), OH$^-$ (blue and purple), and TiO$_2$ lattice oxygen (e_g and t_{2g}, green). The two spectral backgrounds in (C) and (D) are fitted with a cubic function, indicated by gray curves (see also Figure S1). The detailed fitting parameters are presented in Table S2.

exhibits no OH$^-$ signal at this low OH$^-$ concentration; this is also true for a NaOH aqueous solution of the same concentration.[51] Another important difference between the spectra of lower (0.5 M) and higher (5 M) OH$^-$ concentrations is the change of the water O 1s peak width. The full width at half-maximum (fwhm) of the low-concentration spectrum is ~1.6 eV (which is almost the same as for neat liquid water[50]) and increases by 12.5% (0.2 eV wider) for the higher concentration. Qualitatively, such a broadening is in accord with a theoretical finding that hydration of hydroxide affects the electronic structure of water,[52] and it also agrees with a previous experimental and computational PFY-XA study of hydroxide aqueous solution[53] which will be detailed below along with the discussion of Figure 4.

The O 1s PE spectrum of the $[2:1]^{NH_4^+}$ NP solution, shown in Figure 3C, is rather similar to the spectrum of the 5 M NaOH aqueous solution. However, there is an additional small peak from the TiO$_2$ lattice oxygen at 534.8 eV BE, and three additional subtle but significant spectral differences can be observed. (1) The OH$^-$ signal intensity from the NP solution

amounts to almost 70% of that from the 5 M NaOH solution. According to the spectrum of 0.5 M NH$_4$OH (Figure 3B), one would expect to observe no OH$^-$ signal from the $[2:1]^{NH_4^+}$ NP solution, let alone to exhibit the intensity comparable to that of the 5 M NaOH aqueous solution. (2) The fwhm of the water O 1s PE peak is very similar to the one from neat water, and the peak is not broadened unlike in the case of the 5 M NaOH aqueous solution. (3) The OH$^-$ peak position is at slightly smaller (by 0.5 eV) BE compared to the PE spectrum from 5 M NaOH aqueous solution (Figure 3A). All relevant BEs, fwhm, and peak areas are provided in Table S1.

Observation 1 indicates that in the NP solution the number of OH$^-$ significantly exceeds the number that would be provided from 0.3 M concentration, and yet the pH of the $[2:1]^{NH_4^+}$ NP solution is only 7.8. Observations 2 and 3 imply that OH$^-$ species in the NP solution are accommodated in a different chemical environment than the hydrated OH$^-$ in water at basic pH. In our previous work, in the same $[2:1]^{NH_4^+}$ NP aqueous solution,[28] we have reported that water dissociates at the TiO$_2$ NP surface, which can qualitatively explain the increase of OH$^-$ signals (observation 1) in the spectrum. An important consideration is that observation 1 is at odds with the fact that the pH of the $[2:1]^{NH_4^+}$ NP solution is only 7.8. It thus implies that most of the OH$^-$ molecules in the NP solution must be trapped around the TiO$_2$ NPs by the positive Stern layer, forming the diffuse layer of the EDL; these confined OH$^-$ species make no contribution to the pH measurement. Analogous to our previous photoemission study of aqueous-phase TiO$_2$ NPs,[28] we have also measured the $[2:1]^{NH_4^+}$ NP solution with 0.5 M NaOH added (Figure 3D) to show that the intensity of the OH$^-$ peak at 536.3 eV continues to increase, becoming as large as for the 5 M NaOH solution. However, the pH is ~9.8, and the added amount of hydroxide could not produce such signal enhancement. This further corroborates our conclusion that a large amount of OH$^-$ is indeed produced by additional water dissociation at the TiO$_2$ surface. The implications of observations 2 and 3 together with the findings of Figure 3D will be detailed in the following paragraphs, where we acquire additional support from PFY-XA measurements. The latter is indispensable here as it is a bulk-sensitive method, enabling a realistic estimate of the amount of OH$^-$ present in the NP solution.

The O K-edge PFY-XA spectrum of the $[2:1]^{NH_4^+}$ NP solution, with the assistance of the reference PFY-XA spectra of $[1:1]^{Cl^-}$ NP solution, neat water, and 1.5 M NaOH aqueous solution, allows for a quantitative estimation of the OH$^-$ amount in the NP solution. All PFY-XA spectra, shown in Figure 4, were generated by integrating the X-ray emission intensities resulting from valence band to core transitions (O 2p → 1s) following resonant excitation at the O K-edge. Note that the PFY-XA spectrum of the 1.5 M NaOH aqueous solution, shown in Figures 4B and 4D, has been adapted from ref 54. This spectrum helps to quantify the amount of OH$^-$ in the NP solutions, which will be explained later. Figure 4A shows the spectra from the $[2:1]^{NH_4^+}$ NP solution and the $[1:1]^{Cl^-}$ NP solution. Because the latter solution corresponds to the fully Cl$^-$-covered NP surface, water cannot interact with TiO$_2$. Hence, the difference spectrum (dotted curve), $[2:1]^{NH_4^+}$ NP minus $[1:1]^{Cl^-}$ NP, reveals the signal solely due to OH$^-$.
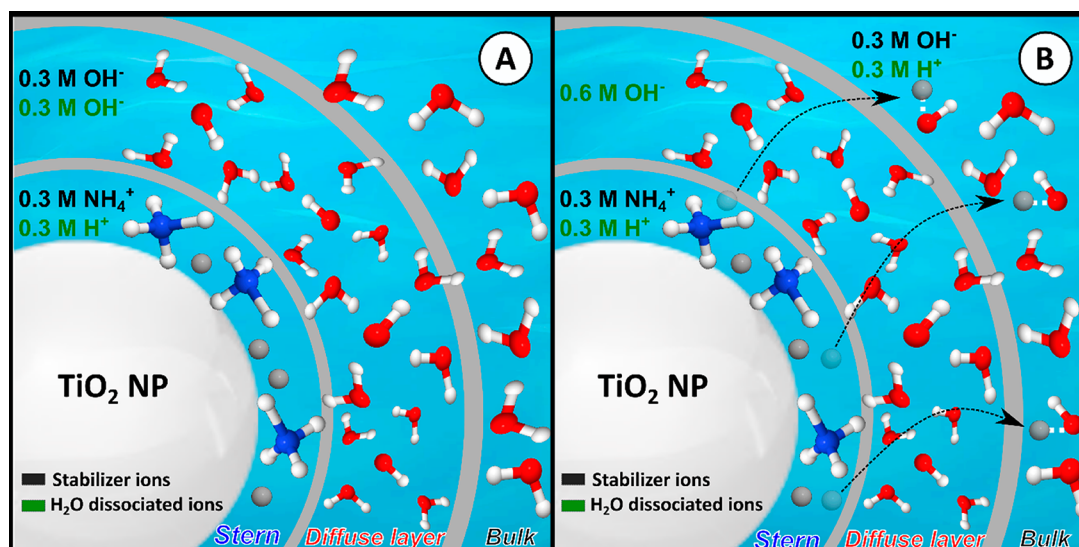
Figure 5. Schematic representation of the charge (NH_4^+, OH^-) distribution in the EDL around a TiO_2 NP in NH_4OH aqueous solution. (A) In scenario A, ~0.3 M H_2O have dissociated at the TiO_2 surface producing H^+ ions that become part of the Stern layer, while the generated 0.3 M OH^- are being accommodated in the diffuse layer. All additional OH^-, also residing within the diffuse layer, originate from the bulk solution (from the 0.3 M NH_4OH stabilizer). (B) Scenario B assumes that 0.6 M H_2O are dissociated which creates 0.6 M OH^- ions in the diffuse layer. Of the corresponding 0.6 M H^+ approximately half of the H^+ are bound to the TiO_2 surface, and the other fraction quickly diffuse into the bulk solution, neutralizing the solution.

We label this signal contribution $OH^-(i^*)$. Then in Figure 4B, we compare $OH^-(i^*)$ with the OH^- signal obtained from the neat 1.5 M NaOH aqueous solution (no NPs contained). For that we subtract the PFY-XA spectrum of neat water (shown in blue) from the one of the NaOH solution (in brown). This difference spectrum is presented at the bottom of Figure 4B. Unlike in Figure 4A, we now observe two contributions, centered at 532.8 and 534.1 eV photon energy, labeled $OH^-(i)$ and $OH^-(ii)$, respectively. These two OH^- contributions have been previously reported for 4 and 6 M KOH aqueous solutions and were attributed, based on computations, to the hydroxide hydration complexes in tricoordinated (tetrahedral-coordinated) $OH^-(H_2O)_3$ and in planar 4-fold-coordinated (hypercoordinated) $OH^-(H_2O)_4$ configurations, respectively.[53] The tetrahedral configuration produces a single pre-edge peak at 532.5 eV photon energy (matching the $OH^-(i)$ peak position in Figure 4B), whereas the hypercoordinated configuration gives rise to a pre-edge peak at 534.5 eV (coinciding with $OH^-(ii)$ in Figure 4B) as well as to $OH^-(i)$.[53] The good agreement between the computed energies for $OH^-(i)$ with the experimental energy of $OH^-(i^*)$ strongly suggests that not only is the OH^- hydration configuration near the NP surface different than in bulk water, but the tricoordinated structure dominates. Note that the occurrence of different OH^- configurations would be qualitatively consistent with the different O 1s BEs found in the NP solution compared to the 5 M NaOH solution (Figures 3A and 3C). Our suggested hydroxide hydration configuration within the EDL is corroborated by a Car–Parrinello molecular dynamics (CPMD) simulation, finding that the fraction of 3- and 4-coordinated structures depends strongly on the OH^- concentration. At low concentration, OH^- ions are surrounded by abundant water molecules, and the $OH^-(H_2O)_4$ hypercoordinated configuration is preferred; the tetrahedral complex $OH^-(H_2O)_3$ quickly (within 2−3 ps) interconverts to $OH^-(H_2O)_4$.[55,56] At high concentration, fewer water molecules are available to coordinate OH^-, making the

$OH^-(H_2O)_3$ configuration more favorable.[57] We argue that the OH^- concentration in the diffuse layer is high, although we have yet to quantify the concentration, and thus the 3-coordinated structure dominates. This interpretation is supported by a nuclear magnetic resonance study of the water molecule distribution around TiO_2 NPs, showing strong confinement of water molecules with low mobility and reactivity within the first few layers above the TiO_2 surface.[58]

The potential cation effect of Na^+ on the hydroxide and water spectra is found to be negligible in this study, even though Na^+ was considered to be bound to hydroxide and water molecules in highly concentrated solutions.[59] We have recently examined the influence of NaI salt on the electronic structure of liquid water by PES and molecular dynamical and quantum chemical calculations[60] and found no significant effect from NaI, up to 8 M concentration, on the water PE spectra. The Na^+ effect on O K-edge XA spectra were investigated previously as well,[61] which showed only 0.09, 0.04, and 0.02 eV energy shifts of the water prepeak at ∼535 eV for NaCl, NaBr, and NaI solutions of 3 M concentrations.

Having characterized the OH^- hydration configurations and their contributions to the PFY-XA spectra, we now quantify the amount of OH^- within the EDL. The O K-edge PFY-XA spectra of $[2:1]^{NH_4^+}$ NP (Figure 4A) and 1.5 M NaOH solutions (Figure 4B) solutions are then fitted with Gaussians, each representing the respective oxygen component, as shown in Figures 4C and 4D. In both cases, the well-known water pre-edge peak at 535.0 eV[62] is presented in blue (unfilled) and is used for intensity normalization; the relative intensity of this signal will be used to estimate the OH^- concentration. In Figure 4C, the two TiO_2 oxygen features at 531.1 and 533.3 eV (green Gaussians), resulting from O 2p orbital hybridization with Ti-3d-derived t_{2g} and e_g orbitals,[63−67] are fitted under the constraints of the same peak positions, widths, and intensity ratio that are obtained from the fitting parameters of the reference PFY-XA spectrum of the $[1:1]^{Cl^-}$ NP solution (no

OH⁻ signal) shown in Figure S1 and Table S2. It is clear that the fitted Gaussian at 532.6 eV (light blue; Figure 4C), which accounts for the OH⁻ signal, is needed to yield a good total fit (red line) of the overall spectrum. The 532.6 eV peak position perfectly matches the position of the computed tetrahedral species $OH^-(H_2O)_3$ (feature OH⁻(i) at 532.5 eV photon energy),[53] in agreement with our above, more qualitative analysis. We notice that in our previous O 1s PE spectroscopy study of TiO_2 NP aqueous solution[28] the obtained PEY-XA spectra exhibit somewhat smaller OH⁻ signal with respect to the water pre-edge intensity. Also, the TiO_2 signal is considerably smaller in the electron-yield measurements. It is this signal-intensity discrimination intrinsic to the (rather surface-sensitive) PES study that does not allow for a quantitative estimate of the relative concentration of the (oxygen) species of interest. In contrast, the signals obtained with bulk-sensitive PFY are argued to quantitatively reflect the total TiO_2 lattice and OH⁻ concentrations in solutions.

In Figure 4D, we present the individual contributions of OH⁻(i) and OH⁻(ii) to the PFY-XA spectrum from 1.5 M NaOH aqueous solution (of Figure 4B), where we are guided by the analysis of ref 53. We first fit the water pre-edge peak (see Figure S1 and its caption) and then include two Gaussian peaks, representing OH⁻(i) and OH⁻(ii). The obtained peak positions (532.8 and 534.1 eV photon energy) are in very good agreement with the energies computed for the hyper-coordinated hydroxide.[53] For estimating the OH⁻ amount in the NP solution, we then compare the Gaussian peak area of tetrahedral (light blue peak in Figure 4C) with the area of hypercoordinated (light violet peaks in Figure 4D) OH⁻ species, from which an ∼0.6 M OH⁻ concentration for the $[2:1]^{NH_4^+}$ NP aqueous solution is derived. Here, we have used the OH⁻-to-H₂O (prepeak) intensity ratio of Figure 4D as a calibration point; see the fitting parameters in Table S2 and related calculation details in the Supporting Information.

We recall that the 0.3 M NH_4OH aqueous solution has a pH of 11.3, whereas the pH of the $[2:1]^{NH_4^+}$ NP solution (prepared in 0.3 M NH_4OH aqueous solution) is only 7.8. Despite this near-neutral pH, the OH⁻ concentration in the NP solution is estimated to be 0.6 M, and almost all these anions are confined within the EDL. Given that at 0.3 M NH_4^+ concentration about half the TiO_2 NP surface sites are covered (estimated from 5.2 ions adsorbed/nm²),[37,38] 0.6 M $OH^-(H_2O)_3$ would be enough to exceed one monolayer coverage, forming the diffuse layer. This raises several questions: (1) how thick is the diffuse layer, (2) what is the origin of the 0.6 M OH⁻ concentration, and (3) what role does the produced H⁺ (from water dissociation) play in this interfacial system? To answer these questions, we propose two scenarios, as schematically presented in Figure 5. Both cases build on the negatively charged NP surface as presented in Figure 1B as well as on the right-hand side of this figure. In this regime, the potential parity is reversed between the Stern layer and the diffuse layer.

Scenario A (Figure 5A) proposes that 0.3 M NH_4OH solution contributes maximum 0.3 M OH⁻ concentration to the diffuse layer (bulk OH⁻ drawn toward the NPs by Coulombic attraction of the Stern layer), and the other 0.3 M OH⁻ is provided by water dissociation at the TiO_2 NP surface. Indeed, our previous liquid microjet PES study of the same $[2:1]^{NH_4^+}$ TiO_2 NP colloidal solution has already shown that OH⁻ can be produced in basic solution from water

dissociation,[28] and subsequent OH⁻ liberation (into the diffuse layer) allows for further dissociation. The amount of OH⁻ that can be accommodated in the diffuse layer depends on the effective charge of the Stern layer, and one crucial question is whether H⁺ (from water dissociation) is part of the Stern layer. As discussed in the Introduction, fast H⁺−OH⁻ recombination is one of the major obstacles limiting the efficiency of water dissociation reactions. In the present scenario, this problem is bypassed by assuming that H⁺ is bound at the TiO_2 surface. This confinement of H⁺ increases the Stern layer charge and keeps the extra negative OH⁻ species stay close, within the diffuse layer. Such a mechanism would be consistent with a previous scanning tunneling microscopy study finding that H⁺ bonds to the oxygen sites of TiO_2 surfaces.[68]

In scenario B (Figure 5B), the 0.6 M OH⁻ concentration is assumed to be completely produced by water dissociation at the TiO_2 NP surfaces. Because of the limited number of anchoring oxygen sites for water on the TiO_2 surface, the excess amount of OH⁻ can be rationalized when assuming that some fraction of H⁺ ions produced at the interface migrate through the diffuse layer and recombine with the original free OH⁻ from the 0.3 M ammonia solution to form water. This latter neutralization would explain the observed relatively low pH 9.8 when adding NaOH to the NP solution (see Figure 3D and respective figure caption). Note that some fraction of H⁺ will inevitably recombine with OH⁻ in the diffuse layer, and the resulting loss of OH⁻ molecules can be replenished because the H⁺ release from the TiO_2 surface vacates adsorption sites for further water dissociation reaction, which in turn generates additional OH⁻ in the diffuse layer. Even if we do not understand the detailed mechanism of such efficient transfer through the diffuse layer (although very thin; discussed below), OH⁻ in the bulk solution, as well as in the diffuse layer, must play an important role in initiating the release of H⁺ from the TiO_2 surface. This dynamical cycle of continuous freeing surface sites for water adsorption, and the subsequent release of H⁺, followed by recombination, will reach an equilibrium once the bulk solution is nearly neutralized. It is worth to note that the different origins of OH⁻ generation proposed in scenarios A and B cannot be experimentally distinguished based on the current experimental data. To accurately understand the mechanism of water dissociation, further studies are required and will help to find ways to continuously extract H⁺ from TiO_2 catalytic sites to generate H₂ for a sustainable catalytic reaction. Such a proposed H⁺ dynamics has been supported by photoelectrochemical cell (PEC) studies under external electric potential.[69−71] Water dissociation was found to occur at the TiO_2 working electrode, followed by H⁺ diffusion through an electrolyte solution to the counter electrode; the nature of the EDL at the working electrode−electrolyte interface was not addressed though.

Finally, the thickness of the diffuse layer is estimated based on the 0.22 nm O−O bond length reported for the $OH^-(H_2O)_n$ complex.[53] The 0.6 M tetrahedral $OH^-(H_2O)_3$ complex derived from the quantitative analysis of the PFY-XA spectra in Figure 4 can then form an at least 0.44 nm thick diffuse layer, corresponding to one complete densely packed monolayer (with 0.3 M NH_4^+ covering half of the TiO_2 NP surface). The actual thickness of the diffuse layer is, however, likely to extend beyond 0.44 nm due to the mobility of $OH^-(H_2O)_3$ ions. Hence, the Debye length should be >0.8 nm; this comprises the >0.44 nm diffuse layer and ∼0.35 nm

Stern layer. Previous electrochemical studies have investigated the interaction force between two electrodes immersed in ionic liquid and in NaCl aqueous solution and obtained a semiparabolic relationship between the interaction force, from which the Debye length can be inferred as a function of electrolyte concentration. The results of ref 72 show that the Debye length reaches an undetectably small value at 0.1 M electrolyte concentration and then goes up to ~1.5 nm for ~2.0 M concentration in the case of NaCl aqueous solution and to ~6 nm for ~2.0 M concentration of ionic liquid solution in propylene.[72] Our >0.8 nm Debye length estimated for the $[2{:}1]^{NH_4^+}$ colloidal solution agrees with this reported Debye length versus concentration relation,[72] although we cannot precisely determine the overall electrolyte concentration.

CONCLUSIONS

We have applied in-situ X-ray spectroscopy to characterize the electric double layer (EDL) around 20 nm TiO_2 NPs dispersed and stabilized in NH_4OH aqueous solution. Our studies thus capture the interaction of bulk electrolyte solution with TiO_2 NP surfaces. By combining PES, PEY-XAS, and PFY-XAS, we find that at low concentration of NH_4^+ stabilizer ions—but still assuring that the NPs do not aggregate—there remains sufficient NP surface area to interact with water. The PES and PEY-XAS measurements at the N 1s and O 1s core levels, along with the measured pH, identify the Stern layer as consisting of NH_4^+ stabilizer ions and the diffuse layer being composed of OH^-. Moreover, the PFY measurements at the O K-edge reveal an unexpectedly large amount of OH^- in the NP aqueous solution (despite near-neutral pH) that can only be explained by water dissociation. These OH^- species are proposed to form an approximately >0.44 nm thick diffuse layer, charge-balanced by an ~0.35 nm Stern layer of NH_4^+. The PFY measurements furthermore strongly suggest a prevailing 3-coordinated OH^- hydration structure, $OH^-(H_2O)_3$, within the diffuse layer—which is not the case for OH^- hydration in bulk solution where the 4-coordinated structure, $OH^-(H_2O)_4$, is more probable. We conclude by proposing two models in which the dissociation product H^+ ions are either completely anchored at the TiO_2—solution interface (scenario A) or partially escape into the bulk solution (scenario B), both consequently preventing the unwanted H^+—OH^- recombination. Scenario B is probably a more realistic description of the dynamics of dissociative water adsorption accompanied by H^+ release and recombination cycle, although elements of both models are likely relevant. The continuous H^+ release from TiO_2 NP surfaces, stimulated by OH^- in the bulk solution or external electric potential applied from electrode, implies efficient water dissociation reactions and sustainable H_2 generation that can be realized in aqueous solutions. In addition, the present work marks an important advance in the spectroscopic characterization of the EDL, including the molecular interactions of aqueous solution with solid surfaces that are relevant for energy-material research. Our method can be readily applied to surfaces other than those studied here.

ASSOCIATED CONTENT

Ⓢ Supporting Information

The Supporting Information is available free of charge at https://pubs.acs.org/doi/10.1021/acsanm.9b01939.

Detailed fitting parameters of the PE spectra in Figure 3, PFY-XA spectra in Figure 4 and the estimation details of OH^- molarity based the fitted peak areas (PDF)

■ AUTHOR INFORMATION

Corresponding Authors
*E-mail hebatallah@fhi-berlin.mpg.de.
*E-mail jie.xiao@helmholtz-berlin.de.

ORCID Ⓘ
Hebatallah Ali: 0000-0001-5037-9889
Bernd Winter: 0000-0002-5597-8888
Jie Xiao: 0000-0002-2320-6111

Author Contributions
All authors planned the experiments, selected the samples, conducted the experiments during multiple beamtimes at BESSY II, and analyzed the data. H.A., B.W., and J.X. wrote the article. All authors have given approval to the final version of the manuscript.

Notes
The authors declare no competing financial interest.

■ REFERENCES

(1) Sato, S.; White, J. Photodecomposition of water over Pt/TiO₂ catalysts. *Chem. Phys. Lett.* **1980**, *72* (1), 83−86.
(2) Serpone, N.; Lawless, D.; Disdier, J.; Herrmann, J.-M. Spectroscopic, photoconductivity, and photocatalytic studies of TiO₂ colloids: naked and with the lattice doped with Cr³⁺, Fe³⁺, and V⁵⁺ cations. *Langmuir* **1994**, *10* (3), 643−652.
(3) Khan, S. U.; Al-Shahry, M.; Ingler, W. B. Efficient photochemical water splitting by a chemically modified n-TiO₂. *Science* **2002**, *297* (5590), 2243−2245.
(4) Diebold, U. The surface science of titanium dioxide. *Surf. Sci. Rep.* **2003**, *48* (5−8), 53−229.
(5) Ni, M.; Leung, M. K.; Leung, D. Y.; Sumathy, K. A review and recent developments in photocatalytic water-splitting using TiO₂ for hydrogen production. *Renewable Sustainable Energy Rev.* **2007**, *11* (3), 401−425.
(6) Di Paola, A.; Bellardita, M.; Palmisano, L. Brookite, the least known TiO₂ photocatalyst. *Catalysts* **2013**, *3* (1), 36−73.
(7) Grätzel, M.; Rotzinger, F. P. The influence of the crystal lattice structure on the conduction band energy of oxides of titanium (IV). *Chem. Phys. Lett.* **1985**, *118* (5), 474−477.

(8) Ola, O.; Maroto-Valer, M. M. Review of material design and reactor engineering on TiO_2 photocatalysis for CO_2 reduction. *J. Photochem. Photobiol., C* **2015**, *24*, 16−42.

(9) Nowotny, J.; Bak, T.; Nowotny, M.; Sheppard, L. TiO_2 surface active sites for water splitting. *J. Phys. Chem. B* **2006**, *110* (37), 18492−18495.

(10) Nowotny, J.; Bak, T.; Nowotny, M.; Sheppard, L. Titanium dioxide for solar-hydrogen IV. Collective and local factors in photoreactivity. *Int. J. Hydrogen Energy* **2007**, *32* (14), 2651−2659.

(11) Walter, M. G.; Warren, E. L.; McKone, J. R.; Boettcher, S. W.; Mi, Q.; Santori, E. A.; Lewis, N. S. Solar water splitting cells. *Chem. Rev. (Washington, DC, U. S.)* **2010**, *110* (11), 6446−6473.

(12) Hashimoto, K.; Irie, H.; Fujishima, A. TiO_2 Photocatalysis: A Historical Overview and Future Prospects. *Jpn. J. Appl. Phys.* **2005**, *44* (12), 8269.

(13) Asahi, R.; Morikawa, T.; Ohwaki, T.; Aoki, K.; Taga, Y. Visible-light photocatalysis in nitrogen-doped titanium oxides. *Science* **2001**, *293* (5528), 269−71.

(14) Nowotny, J.; Sorrell, C.; Bak, T.; Sheppard, L. Solar-hydrogen: Unresolved problems in solid-state science. *Sol. Energy* **2005**, *78* (5), 593−602.

(15) Helmholtz, H. v. Ueber einige Gesetze der Vertheilung elektrischer Ströme in körperlichen Leitern, mit Anwendung auf die thierisch-elektrischen Versuche (Schluss.). *Ann. Phys.* **1853**, *165* (7), 353−377.

(16) Chapman, D. L. LI. A contribution to the theory of electrocapillarity. *London, Edinburgh, and Dublin philosophical magazine and journal of science* **1913**, *25* (148), 475−481.

(17) Gouy, M. Sur la constitution de la charge électrique à la surface d'un électrolyte. *J. Phys. Theor. Appl.* **1910**, *9* (1), 457−468.

(18) Stern, O. The theory of the electrolytic double-layer. *Z. Elektrochem.* **1924**, *30* (508), 1014−1020.

(19) Polte, J. Fundamental growth principles of colloidal metal nanoparticles−a new perspective. *CrystEngComm* **2015**, *17* (36), 6809−6830.

(20) Guo, D.; Xie, G.; Luo, J. Mechanical properties of nanoparticles: basics and applications. *J. Phys. D: Appl. Phys.* **2014**, *47* (1), No. 013001.

(21) Elimelech, M.; Gregory, J.; Jia, X. *Particle Deposition and Aggregation: Measurement, Modelling and Simulation*; Butterworth-Heinemann: 2013.

(22) Zhao, Z.; Li, Z.; Zou, Z. Structure and properties of water on the anatase TiO_2 (101) surface: from single-molecule adsorption to interface formation. *J. Phys. Chem. C* **2012**, *116* (20), 11054−11061.

(23) Fenter, P.; Cheng, L.; Rihs, S.; Machesky, M.; Bedzyk, M. J.; Sturchio, N. Electrical double-layer structure at the rutile−water interface as observed in situ with small-period X-ray standing waves. *J. Colloid Interface Sci.* **2000**, *225* (1), 154−165.

(24) Předota, M.; Bandura, A.; Cummings, P.; Kubicki, J.; Wesolowski, D.; Chialvo, A.; Machesky, M. Electric double layer at the rutile (110) surface. 1. Structure of surfaces and interfacial water from molecular dynamics by use of ab initio potentials. *J. Phys. Chem. B* **2004**, *108* (32), 12049−12060.

(25) Cheng, J.; Sprik, M. The electric double layer at a rutile TiO_2 water interface modelled using density functional theory based molecular dynamics simulation. *J. Phys.: Condens. Matter* **2014**, *26* (24), 244108.

(26) Favaro, M.; Jeong, B.; Ross, P. N.; Yano, J.; Hussain, Z.; Liu, Z.; Crumlin, E. J. Unravelling the electrochemical double layer by direct probing of the solid/liquid interface. *Nat. Commun.* **2016**, *7*, 12695.

(27) Rubasinghege, G.; Grassian, V. H. Role(s) of adsorbed water in the surface chemistry of environmental interfaces. *Chem. Commun. (Cambridge, U. K.)* **2013**, *49* (30), 3071−3094.

(28) Ali, H.; Seidel, R.; Bergmann, A.; Winter, B. Electronic structure of aqueous-phase anatase titanium dioxide nanoparticles probed by liquid jet photoelectron spectroscopy. *J. Mater. Chem. A* **2019**, *7*, 6665−6675.

(29) Seidel, R.; Pohl, M. N.; Ali, H.; Winter, B.; Aziz, E. F. Advances in liquid phase soft-x-ray photoemission spectroscopy: A new experimental setup at BESSY II. *Rev. Sci. Instrum.* **2017**, *88* (7), No. 073107.

(30) Aziz, E. F.; Xiao, J.; Golnak, R.; Tesch, M. LiXEdrom: High Energy Resolution RIXS Station dedicated to Liquid Investigation at BESSY II. *JLSRF* **2016**, *2*, 80.

(31) Winter, B. Liquid microjet for photoelectron spectroscopy. *Nucl. Instrum. Methods Phys. Res., Sect. A* **2009**, *601* (1), 139−150.

(32) Brown, M. A.; Beloqui Redondo, A.; Sterrer, M.; Winter, B.; Pacchioni, G.; Abbas, Z.; van Bokhoven, J. A. Measure of surface potential at the aqueous−oxide nanoparticle interface by XPS from a liquid microjet. *Nano Lett.* **2013**, *13* (11), 5403−5407.

(33) Makowski, M. J.; Galhenage, R. P.; Langford, J.; Hemminger, J. C. Liquid-Jet X-ray Photoelectron Spectra of TiO_2 Nanoparticles in an Aqueous Electrolyte Solution. *J. Phys. Chem. Lett.* **2016**, *7* (9), 1732−1735.

(34) Brown, M. A.; Seidel, R.; Thürmer, S.; Faubel, M.; Hemminger, J. C.; van Bokhoven, J. A.; Winter, B.; Sterrer, M. Electronic structure of sub-10 nm colloidal silica nanoparticles measured by in situ photoelectron spectroscopy at the aqueous-solid interface. *Phys. Chem. Chem. Phys.* **2011**, *13* (28), 12720−12723.

(35) Ali, H.; Seidel, R.; Pohl, M. N.; Winter, B. Molecular species forming at the α-Fe_2O_3 nanoparticle−aqueous solution interface. *Chem. Sci.* **2018**, *9* (19), 4511−4523.

(36) Jordan, I.; Redondo, A. B.; Brown, M. A.; Fodor, D.; Staniuk, M.; Kleibert, A.; Wörner, H. J.; Giorgi, J. B.; van Bokhoven, J. A. Non-uniform spatial distribution of tin oxide (SnO_2) nanoparticles at the air−water interface. *Chem. Commun. (Cambridge, U. K.)* **2014**, *50* (32), 4242−4244.

(37) Ketteler, G.; Yamamoto, S.; Bluhm, H.; Andersson, K.; Starr, D. E.; Ogletree, D. F.; Ogasawara, H.; Nilsson, A.; Salmeron, M. The nature of water nucleation sites on TiO_2 (110) surfaces revealed by ambient pressure X-ray photoelectron spectroscopy. *J. Phys. Chem. C* **2007**, *111* (23), 8278−8282.

(38) Walle, L.; Borg, A.; Johansson, E.; Plogmaker, S.; Rensmo, H.; Uvdal, P.; Sandell, A. Mixed dissociative and molecular water adsorption on anatase TiO_2 (101). *J. Phys. Chem. C* **2011**, *115* (19), 9545−9550.

(39) Emerson, K.; Russo, R. C.; Lund, R. E.; Thurston, R. V. Aqueous ammonia equilibrium calculations: effect of pH and temperature. *J. Fish. Res. Board Can.* **1975**, *32* (12), 2379−2383.

(40) Bates, R. G.; Pinching, G. Acidic dissociation constant of ammonium ion at 0 to 50 C, and the base strength of ammonia. *Journal of Research of the National Bureau of Standards* **1949**, *42*, 419−430.

(41) Golnak, R.; Bokarev, S. I.; Seidel, R.; Xiao, J.; Grell, G.; Atak, K.; Unger, I.; Thurmer, S.; Aziz, S. G.; Kuhn, O.; Winter, B.; Aziz, E. F. Joint Analysis of Radiative and Non-Radiative Electronic Relaxation Upon X-ray Irradiation of Transition Metal Aqueous Solutions. *Sci. Rep.* **2016**, *6*, 2808−2814.

(42) Weinhardt, L.; Ertan, E.; Iannuzzi, M.; Weigand, M.; Fuchs, O.; Bar, M.; Blum, M.; Denlinger, J. D.; Yang, W.; Umbach, E.; Odelius, M.; Heske, C. Probing hydrogen bonding orbitals: resonant inelastic soft X-ray scattering of aqueous NH_3. *Phys. Chem. Chem. Phys.* **2015**, *17* (40), 27145−27153.

(43) Perry, R.; Chilton, C. *Chemical Engineers' Handbook*; McGraw-Hill: New York, 1973; Section 3.

(44) Unger, I.; Hollas, D.; Seidel, R.; Thürmer, S.; Aziz, E. F.; Slavicek, P.; Winter, B. Control of X-ray induced electron and nuclear dynamics in ammonia and glycine aqueous solution via hydrogen bonding. *J. Phys. Chem. B* **2015**, *119* (33), 10750−10759.

(45) Ogunremi, T.; Cutler, J.; Christensen, C.; Sparks, C. In X-ray Absorption Spectroscopic analysis of raw and processed hog manure, Soils and Crops Workshop, 2007.

(46) Leinweber, P.; Kruse, J.; Walley, F. L.; Gillespie, A.; Eckhardt, K.-U.; Blyth, R. I.; Regier, T. Nitrogen K-edge XANES−an overview of reference compounds used to identify unknown 'organic nitrogen in environmental samples. *J. Synchrotron Radiat.* **2007**, *14* (6), 500−511.

(47) Seidel, R.; Winter, B.; Bradforth, S. E. Valence electronic structure of aqueous solutions: Insights from photoelectron spectroscopy. *Annu. Rev. Phys. Chem.* **2016**, *67*, 283−305.

(48) Sidey, V. On the effective ionic radii for ammonium. *Acta Crystallogr., Sect. B: Struct. Sci., Cryst. Eng. Mater.* **2016**, *72* (4), 626−633.

(49) Brown, M. A.; Faubel, M.; Winter, B. X-ray photo-and resonant Auger-electron spectroscopy studies of liquid water and aqueous solutions. *Annu. Rep. Prog. Chem., Sect. C: Phys. Chem.* **2009**, *105*, 174−212.

(50) Winter, B.; Aziz, E. F.; Hergenhahn, U.; Faubel, M.; Hertel, I. V. Hydrogen bonds in liquid water studied by photoelectron spectroscopy. *J. Chem. Phys.* **2007**, *126* (12), 124504.

(51) Winter, B.; Faubel, M.; Vácha, R.; Jungwirth, P. Behavior of hydroxide at the water/vapor interface. *Chem. Phys. Lett.* **2009**, *474* (4−6), 241−247.

(52) Tuckerman, M. E.; Chandra, A.; Marx, D. Structure and dynamics of OH$^-$(aq). *Acc. Chem. Res.* **2006**, *39* (2), 151−158.

(53) Cappa, C. D.; Smith, J. D.; Messer, B. M.; Cohen, R. C.; Saykally, R. J. Nature of the aqueous hydroxide ion probed by X-ray absorption spectroscopy. *J. Phys. Chem. A* **2007**, *111* (22), 4776−4785.

(54) Blum, M. Electronic and Chemical Properties of Liquids and Solutions, Universität Würzburg, 2009.

(55) Tuckerman, M.; Laasonen, K.; Sprik, M.; Parrinello, M. Ab initio molecular dynamics simulation of the solvation and transport of hydronium and hydroxyl ions in water. *J. Chem. Phys.* **1995**, *103* (1), 150−161.

(56) Asthagiri, D.; Pratt, L. R.; Kress, J. D.; Gomez, M. A. Hydration and mobility of HO$^-$(aq). *Proc. Natl. Acad. Sci. U. S. A.* **2004**, *101* (19), 7229−7233.

(57) Chen, B.; Park, J. M.; Ivanov, I.; Tabacchi, G.; Klein, M. L.; Parrinello, M. First-principles study of aqueous hydroxide solutions. *J. Am. Chem. Soc.* **2002**, *124* (29), 8534−8535.

(58) Zhu, L.; Gu, Q.; Sun, P.; Chen, W.; Wang, X.; Xue, G. Characterization of the mobility and reactivity of water molecules on TiO$_2$ nanoparticles by ^{1}H solid-state nuclear magnetic resonance. *ACS Appl. Mater. Interfaces* **2013**, *5* (20), 10352−10356.

(59) Abbas, Z.; Ahlberg, E.; Nordholm, S. Monte Carlo Simulations of Salt Solutions: Exploring the Validity of Primitive Models. *J. Phys. Chem. B* **2009**, *113* (17), 5905−5916.

(60) Pohl, M. N.; Muchová, E.; Seidel, R.; Ali, H.; Sršeň, Š.; Wilkinson, I.; Winter, B.; Slavíček, P. Do water's electrons care about electrolytes? *Chem. Sci.* **2019**, *10* (3), 848−865.

(61) Nagasaka, M.; Yuzawa, H.; Kosugi, N. Interaction between water and alkali metal ions and its temperature dependence revealed by oxygen K-edge x-ray absorption spectroscopy. *J. Phys. Chem. B* **2017**, *121* (48), 10957−10964.

(62) Winter, B.; Hergenhahn, U.; Faubel, M.; Björneholm, O.; Hertel, I. V. Hydrogen bonding in liquid water probed by resonant Auger-electron spectroscopy. *J. Chem. Phys.* **2007**, *127* (9), No. 094501.

(63) Thomas, A. G.; Flavell, W. R.; Mallick, A. K.; Kumarasinghe, A. R.; Tsoutsou, D.; Khan, N.; Chatwin, C.; Rayner, S.; Smith, G. C.; Stockbauer, R. L.; Warren, S.; Johal, T. K.; Patel, S.; Holland, D.; Taleb, A.; Wiame, F. Comparison of the electronic structure of anatase and rutile TiO$_2$ single-crystal surfaces using resonant photoemission and X-ray absorption spectroscopy. *Phys. Rev. B: Condens. Matter Mater. Phys.* **2007**, *75* (3), No. 035105.

(64) Vayssieres, L.; Persson, C.; Guo, J.-H. Size effect on the conduction band orbital character of anatase TiO$_2$ nanocrystals. *Appl. Phys. Lett.* **2011**, *99* (18), 183101.

(65) Mosquera, A. A.; Endrino, J. L.; Albella, J. M. XANES observations of the inhibition and promotion of anatase and rutile phases in silver containing films. *J. Anal. At. Spectrom.* **2014**, *29* (4), 736−742.

(66) Ruus, R.; Kikas, A.; Saar, A.; Ausmees, A.; Nommiste, E.; Aarik, J.; Aidla, A.; Uustare, T.; Martinson, I. Ti 2p and O 1s X-ray absorption of TiO$_2$ polymorphs. *Solid State Commun.* **1997**, *104* (4), 199−203.

(67) De Groot, F. M. F.; Grioni, M.; Fuggle, J. C.; Ghijsen, J.; Sawatzky, G. A.; Petersen, H. Oxygen 1s x-ray-absorption edges of transition-metal oxides. *Phys. Rev. B: Condens. Matter Mater. Phys.* **1989**, *40* (8), 5715−5723.

(68) Balajka, J.; Hines, M. A.; DeBenedetti, W. J.; Komora, M.; Pavelec, J.; Schmid, M.; Diebold, U. High-affinity adsorption leads to molecularly ordered interfaces on TiO$_2$ in air and solution. *Science* **2018**, *361* (6404), 786−789.

(69) Zaleska-Medynska, A. *Metal Oxide-based Photocatalysis: Fundamentals and Prospects for Application*; Elsevier: 2018.

(70) Wang, D.; Cao, G. *Nanomaterials for Energy Conversion and Storage*; World Scientific: 2018.

(71) Minggu, L. J.; Daud, W. R. W.; Kassim, M. B. An overview of photocells and photoreactors for photoelectrochemical water splitting. *Int. J. Hydrogen Energy* **2010**, *35* (11), 5233−5244.

(72) Smith, A. M.; Lee, A. A.; Perkin, S. The electrostatic screening length in concentrated electrolytes increases with concentration. *J. Phys. Chem. Lett.* **2016**, *7* (12), 2157−2163.